

Strong correlation effects and optical conductivity in electron doped cuprates

Tanmoy Das, R. S. Markiewicz, and A. Bansil

Physics Department, Northeastern University, Boston MA 02115, USA

(Dated: February 10, 2022)

We demonstrate that most features ascribed to strong correlation effects in various spectroscopies of the cuprates are captured by a calculation of the self-energy incorporating effects of spin and charge fluctuations. The self energy is calculated over the full doping range of electron-doped cuprates from half filling to the overdoped system. The spectral function reveals four subbands, two widely split incoherent bands representing the remnant of the split Hubbard bands, and two additional coherent, spin- and charge-dressed in-gap bands split by a spin-density wave, which collapses in the overdoped regime. The incoherent features persist to high doping, producing a remnant Mott gap in the optical spectra, while transitions between the in-gap states lead to pseudogap features in the mid-infrared.

PACS numbers: 74.25.Gz, 74.72.-h, 74.20.Mn, 74.25.Jb

A key issue in cuprate physics is to understand the routes through which cuprates evolve from a ‘Mott’ insulator at half filling to a high- T_c superconductor at optimal doping. Underdoped cuprates show the presence of a ‘pseudogap’ or a region of depleted density of states extending to several hundred meV’s around the Fermi energy and thus are very unconventional, but the overdoped system behaves closer to a normal Fermi liquid and is thus amenable to a largely conventional description. Along these lines, evidence of small Fermi surface pockets[1] has been reported in the underdoped regime, while in overdoped $\text{Ti}_2\text{Ba}_2\text{CuO}_{6+\delta}$, a large, three-dimensional Fermi surface consistent with LDA band structure calculations[2] is observed. In sharp contrast, optical studies point to a far more complex and puzzling picture in that even in the overdoped case, an absorption peak characteristic of the Mott gap continues to persist[3, 4] in the spectra, suggesting that doping introduces new in-gap states in which the pseudogap physics resides, but that otherwise the Mott gap persists at all dopings. Here we show that a relatively simple and transparent model of the electronic self energy, where the quasiparticles are dressed with spin wave excitations, captures the key experimentally observed features of the remarkable doping evolution in optical and other spectroscopies, including in particular the persistence of the Mott gap in the overdoped regime. Our self-energy is also in good accord with quantum Monte Carlo computations in the parameter regimes where the latter are available.

We evaluate the self-energy Σ as a convolution over the green function G and the interaction $W \sim U^2\chi$ (including both spin and charge contributions) as [5],

$$\Sigma(\vec{k}, \sigma, i\omega_n) = \frac{3}{2}U^2 \sum_{\vec{q}, \sigma'} \int_{-\infty}^{\infty} \frac{d\omega_p}{2\pi} G(\vec{k} + \vec{q}, \sigma', \omega_n + \omega_p) \Gamma(\vec{k}, \vec{q}, \omega_n, \omega_p) \text{Im}[\chi^{\sigma\sigma'}(\vec{q}, \omega_p)], \quad (1)$$

where σ is the spin index and the prime over the \vec{q} summation means that the summation is restricted to

the magnetic Brillouin zone. In the underdoped region, the pseudogap is modeled by an antiferromagnetic (AFM) order parameter, resulting in G , χ and Σ becoming 2×2 tensors[6]. We define a total self-energy as $\Sigma^t = US\tilde{\tau}_1 + \Sigma$, where $\tilde{\tau}_1$ is the Pauli matrix along the x -direction and US is the AFM gap defined below. The self-energy Σ^t contains essentially two energy scales: (i) it gives rise to the SDW with an additional renormalization of the overall quasiparticle dispersions in the low energy region, and (ii) at higher energies it produces the Hubbard bands. We use a modified self-consistent scheme, referred to as quasiparticle- GW (QP- GW)-scheme in which G and W are calculated from an approximate self-energy $\Sigma_0^t(\omega) = US\tilde{\tau}_1 + (1 - Z^{-1})\omega\tilde{1}$, where the renormalization factor Z is adjusted self-consistently to match the self-energy Σ^t at low energy.[7, 8]

We find that near optimal doping spin waves[7, 8, 9, 10, 11] dress the quasiparticles into a coherent *in-gap state*, while the incoherent high-energy features are remnants of the upper and lower Hubbard bands (U/LHBs)[12]. With underdoping the in-gap state develops into a spin density wave (SDW) state which opens a gap between the upper and lower magnetic bands (U/LMBs). The model also describes the high-energy kink or the waterfall effect seen in the electronic dispersion[13] as the crossover between coherent and incoherent features.

The present calculations are restricted to the electron-doped cuprates in order to avoid possible complications of nanoscale phase separation. The self-energy Σ_0^t splits the LDA-band, $\xi_{\vec{k}}$ (modelled by tight-binding (TB) parameters[7]) into renormalized UMB ($\nu = +$) and LMB ($\nu = -$):

$$E_{\vec{k}}^{\nu} = Z \left(\xi_{\vec{k}}^{\pm} \pm \sqrt{(\xi_{\vec{k}}^{\pm})^2 + (US)^2} \right), \quad (2)$$

where $\xi_{\vec{k}}^{\pm} = (\xi_{\vec{k}} \pm \xi_{\vec{k}+\vec{Q}})/2$. The AFM magnetization S at $\vec{Q} = (\pi, \pi)$ is calculated self-consistently at each doping, assuming a doping dependent U . [14] In the present formalism U is renormalized by Z . The doping depen-

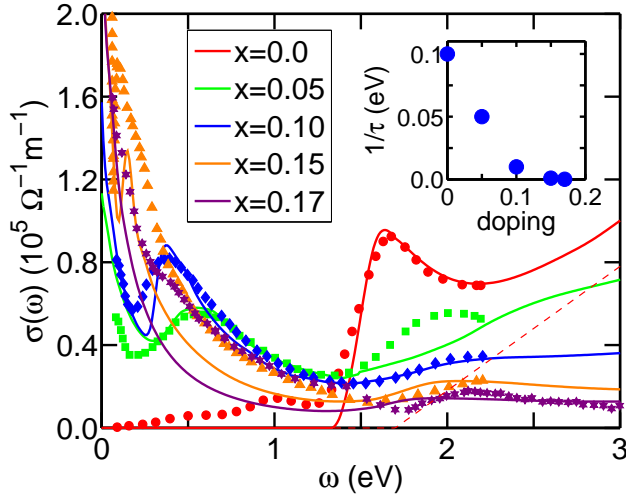


FIG. 1: (color online) Calculated optical conductivity (solid lines) compared with experiment (symbols of same color) for dopings $x = 0.0$ to $x = 0.15$ as taken from Ref. 3 and for $x = 0.17$ from Ref. 4. Experimental data for $x = 0.17$ is subtracted by a background contribution to match the other data set. The dashed line gives the background contribution added to the theoretical spectrum at $x = 0$. inset: Inferred doping dependence of the scattering rate.

gency of U is chosen such that ZU reproduces the pseudogap in both angle-resolved photoemission spectroscopy (ARPES) and optical spectra, while x , S , and Z are determined self-consistently.[15] Finally, the vertex correction $\Gamma(\vec{k}, \vec{q}, \omega, \omega_p)$ in Eq. 1 is taken as its first order approximation (Ward's identity) as $\Gamma(\vec{k}, \vec{q}, \omega, \omega_p) = 1/Z$. Since the k -dependence of Σ is weak, we further simplify the calculation by assuming a k -independent Σ , which we calculate at a representative point $k = (\pi/2, \pi/2)$.

We begin by discussing the optical spectra of Fig. 1. The frequency dependent optical conductivity, $\sigma(\omega)$, is calculated using standard linear response theory in the AFM state,[16] for the full doping range from the half-filled state to the quantum critical point (QCP) in the overdoped region. A very good level of accord is seen with the experimental results[3, 4]. To fit the Drude conductivity, we have introduced an impurity scattering rate τ which is found to have a strong doping dependence (inset). At high energy we include a doping-dependent background contribution, presumably associated with interband transitions to higher-lying bands not included in the present calculations. We have used the same energy-dependence of the background for all dopings with an intensity that decreases smoothly with doping. The red dashed line in Fig. 1 shows this interband contribution for the $x = 0.0$ spectrum.

Interestingly, the spectra show a nearly isosbetic (equal absorption) point near 1.4 eV, consistent with the experimental behavior. The doping evolution is completely different on opposite sides of this isosbetic point. Above this

point the spectrum is dominated by a broad hump feature above 1.5 eV, a signature of the Mott gap. At half-filling, only this feature is present and the optical spectrum shows an insulating gap whose energy, structure, and intensity match remarkably with measurements[3]. As doping increases the high energy peak shifts to higher energy and broadens.

Below the isosbetic point there is little spectral weight at half filling, but as doping increases spectral weight is gradually transferred from the higher energy region to the mid-infrared (MIR) one. The lower energy spectrum is associated with a Drude peak related to intraband transitions and a mid-infrared peak associated with transitions across the magnetic gap [the pseudogap for the electron-doped cuprates]. With doping, this peak shifts to lower energy as the magnetic gap collapses and gradually sharpens due to the doping dependent scattering rate, see inset to Fig. 1. Note that at $x = 0.17$, when the pseudogap has collapsed, Mott-gap features still persist in the spectrum. The present mean-field calculation overestimates the Néel temperature T_N , but this can be corrected by including critical fluctuations, *grave a la* the Mermin-Wagner theorem[17].

The origin of these features can be understood by looking at the doping dependence of the momentum-resolved spectral weight in Fig. 2. In the overdoped case in Fig. 2(e), a kink due to the bosonic coupling reproduces the waterfall effect below E_F , with a corresponding effect above E_F , splitting the spectrum into an effective three-band behavior, with UHB, LHB, and in-gap states. The features in the optical spectra are associated with transitions between these bands: The residual Mott gap arises from the transition from the LMB to the incoherent UHB [or from LHB to UMB], while the Drude term is associated with intraband transitions near the Fermi level. At lower doping an AFM gap opens in the coherent in-gap states[18], leading to the UMB/LMB splitting and a four band behavior similar to that seen in QMC cluster calculations[19]. Consistent with the QMC calculations, the coherent in-gap bands are dressed by magnetic quasiparticles. As the magnetic gap opens, the MIR feature in the optical spectra, being associated with transitions across this gap, shifts to higher energy.

The quality of self-consistency of our scheme can be assessed by noting that the final coherent bands have nearly the same dispersion as the Σ_0 -dressed ones (gold lines) used as input to obtain the self-energy. The doping dependence of the two coherent magnetic bands is in excellent agreement with experiments[20] and earlier mean field calculations[14], and captures the incoherent weight (the UHB/LHBs) at higher energies seen experimentally. Note that the incoherent weight is concentrated near the top and bottom of the bare LDA bands, leading to a nearly doping independent UHB-LHB splitting.

Further insight is provided by Fig. 3(a), which compares the full QP-GW DOS (blue line) and the Σ_0 -

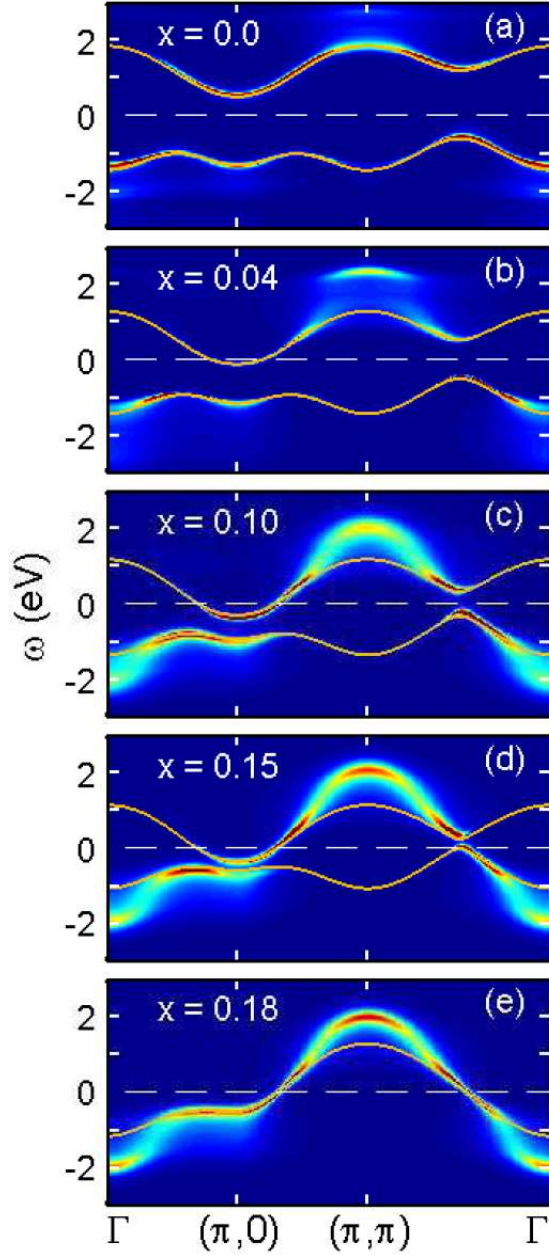


FIG. 2: (color online) Spectral intensity as a function of ω along the high-symmetry lines for several dopings (at temperature $T = 0$). Blue to red color map gives the minimum to maximum intensity. In each panel, the gold lines represent the renormalized magnetic bands (Σ_0 -dressed).

dressed quasiparticle DOS (red line), normalized to the same peak height, for a representative doping $x = 0.04$. The good agreement between various computations over most of the energy range indicates the high degree of self-consistency in the self-energy. The dressed DOS shows four well-separated peaks. A clear leading edge gap of ~ 0.3 eV (~ 1 eV at $x = 0$) can be seen. A gap persists at higher doping up to $x = 0.18$ (Fig. 1), although it is obscured in the DOS by band overlap. The importance

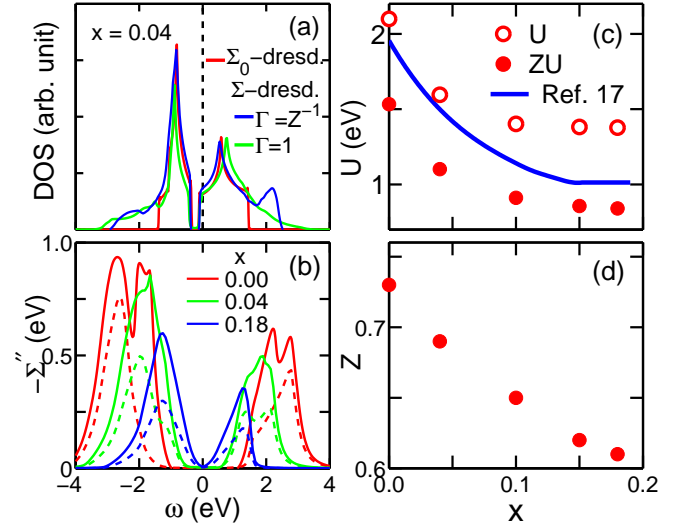


FIG. 3: (color online) (a) The QP-GW DOS (blue lines) is compared with Σ_0 -dressed DOS (red lines) calculated at $T = 0$. The green lines show the DOS without the vertex correction. (b) Solid lines give the imaginary part of the total self-energy, while the dashed lines give the corresponding charge contributions. (c) Doping dependence of self-consistent values of U and ZU is compared with earlier mean field results[14, 21]. (d) Renormalization factor Z decreases linearly with doping.

of the vertex correction is illustrated by the green line in Fig. 3(a), which shows that setting $\Gamma = 1$ reduces the weight in the U/LHBs.

Figure 3(b) shows how the calculated imaginary self-energy Σ'' evolves with doping. The solid lines give the total Σ'' , with the corresponding dashed lines giving the charge contribution. [$\Sigma_{\text{spin}} = \Sigma_{\text{total}} - \Sigma_{\text{charge}}$ is not shown]. In the underdoped region the extra splitting at high energies in the self energy is related to spin-charge separation. The spin response is significant at low energy for all doping but the charge contribution is nearly zero in the low energy region for the lower doping and becomes finite only at higher energies above ~ 3 eV. As doping increases, the charge response moves toward the Fermi level and increases in contribution to its total value. At $x = 18\%$, when the AFM gap vanishes, the charge and spin susceptibility become equal. Note that the broadening of the self-energy evident in Fig. 3(b) is reflected in the increasing broadening of the Mott gap feature with doping. The shift of the peak in the imaginary part of the self-energy towards E_F in Fig. 3(b) reflects the doping dependence of the MIR feature in Fig. 1.

Fig. 3(c) describes the doping dependence of U . Although the renormalized Hubbard parameter ZU follows almost the same doping dependence as in mean field calculations[14, 21], the bare U displays considerably weaker doping dependence away from half-filling. The renormalization factor Z in Fig. 3(d) actually increases with underdoping.[22] This can be readily understood.

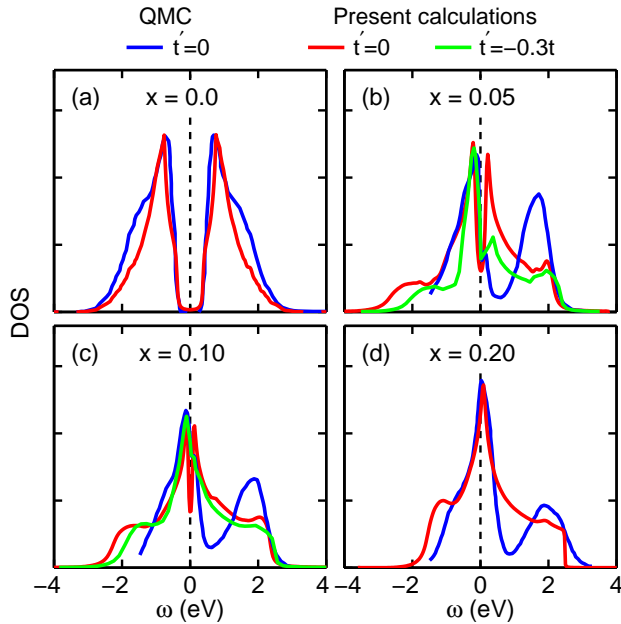


FIG. 4: (color online) The computed DOS at various dopings are compared with the corresponding QMC results (blue lines) for $x = 0.0$ [23] and for $x = 0.05$ to $x = 0.20$ [24]. The red lines in each panel give our result for $t' = 0$, whereas the green lines in (b) and (c) are for $t' = -0.3t$.

As we lower doping, the AFM gap increases leading to a decrease of the spectral weight near the Fermi level. This causes a reduction of the real part of the self-energy, shifting the peak in Σ' towards higher energy. The resulting slope decrease leads to a larger Z .

Existing QMC calculations on the cuprates generally employ simpler hopping parameter sets, so we have repeated our calculations with the same band parameters for a quantitative comparison in Fig. 4. All the QMC results (blue lines) are obtained for $t' = 0$, $U = 8t$ with a momentum dependent self-energy correction[23, 24]. We have obtained the corresponding DOSs (red lines) for $t' = 0$ for Σ calculated at a fixed momentum of $k = (\pi/2, \pi/2)$, using a doping dependent renormalized U (ZU) very similar to the one found for the electron doped case in Fig. 3(c). [Note that the QMC automatically generates a renormalized U]. Our result reproduces the QMC very well for $x = 0$ in Fig. 4(a) where a prominent electron-hole symmetry is observed. At higher doping, the QMC results show a relatively smaller coherent peak above the Fermi level, whereas our result continues to exhibit near electron-hole symmetry in the in-gap region as might be expected for $t' = 0$ dispersion. We can mimic a momentum dependent self-energy by including $t' = -0.3t$, and find that this provides better agreement with the QMC results as shown by the green lines in Figs. 4(b) and 4(c). Finally, at $x = 0.20$, the pseudogap collapses and our result with $t' = 0$ agrees very well with the QMC in Fig. 4(d). As might be expected from

our approximate self-energy calculation, the weight of the UHB is generally underestimated.

In summary, we find that spin-wave dressing of the quasiparticles explains the incoherent U/LHB features seen in various experiments including the recent experiments observing waterfall effects in the cuprate spectra. The self-energy corrections not only renormalize the large widths of the LDA dispersions but also restore the residual incoherent spectral weight associated with U/LHBs. In the underdoped regime, we show that the coherent in-gap bands reproduce both the four-band behavior seen in quantum cluster calculations and the magnetic gap collapse found in the mean-field calculations and a variety of experiments. The puzzling persistence of the Mott gap in optical spectra, even as the magnetic gap collapses, is thus reconciled. The fact that our calculations work so well confirms that the cuprates can be understood within the intermediate coupling regime, with U much less than twice the bandwidth.[25].

We thank Mark Jarrell for important conversations. This work is supported by the U.S.D.O.E, Basic Energy Sciences, contracts DE-FG02-07ER46352 and DE-AC03-76SF00098, and benefited from the allocation of super-computer time at NERSC and Northeastern University's Advanced Scientific Computation Center (ASCC).

-
- [1] N. Doiron-Leyraud *et al.* Nature (London) **447**, 565 (2007).
 - [2] N. E. Hussey *et al.* Nature **425**, 814817 (2003).
 - [3] Y. Onose *et al.*, Phys. Rev. B. **69**, 024504 (2004).
 - [4] S. Uchida *et al.*, Phys. Rev. B **43**, 7942 (1991).
 - [5] G. Vignale and M. R. Hedayati, Phys. Rev. B., **42**, 786 (1990).
 - [6] J. R. Schrieffer, X. G. Wen, and S. C. Zhang, Phys. Rev. B. **39**, 11663 (1989). A. V. Chubukov and D. M. Frenkel, Phys. Rev. B. **46**, 11884 (1992).
 - [7] R. S. Markiewicz, S. Sahrakorpi, and A. Bansil, Phys. Rev. B **76**, 174514 (2007).
 - [8] R. S. Markiewicz and A. Bansil, Phys. Rev. B **75**, 020508 (2007).
 - [9] A. Macridin *et al.*, Phys. Rev. Lett. **97**, 036401 (2006).
 - [10] B. Moritz *et al.* arXiv:0807.3359.
 - [11] While the low-energy carriers are mainly dressed by electronic excitations in the magnetic channel[7, 9], the charge channel can also contribute[8].
 - [12] In reality, the Mott physics lies at a higher energy, comparable to the bonding-antibonding separation of the CuO₂-hybridized bands, and the bands we refer to as U/LHB are the incoherent high energy tails of the antibonding (LDA) band.
 - [13] F. Ronning *et al.* Phys. Rev. B **71**, 094518 (2005); J. Graf *et al.*, Phys. Rev. Lett. **98**, 067004 (2007); J. Graf *et al.*, Physica C **460**, 194 (2007); Z.-H. Pan *et al.* arXiv:cond-mat/0610442 (unpublished).
 - [14] C. Kusko *et al.*, Phys. Rev. B. **66**, 140513(R) (2002).
 - [15] Tanmoy Das, R. S. Markiewicz, and A. Bansil, Phys. Rev. B **77**, 134516 (2008) .

- [16] P. B. Allen, arXiv:cond-mat/0407777 (unpublished).
- [17] R.S. Markiewicz, Phys. Rev. B **70**, 174518 (2004).
- [18] We use a single renormalisation factor for both bands at all dopings.
- [19] C. Gröber, R. Eder, and W. Hanke, Phys. Rev. B **62**, 4336 (2000).
- [20] N.P. Armitage, *et al.*, Phys. Rev. Lett. **88**, 257001 (2002).
- [21] Tanmoy Das, R. S. Markiewicz and A. Bansil, Phys. Rev. Lett. **98**, 197004 (2007).
- [22] Recall that this Z parameter represents an average renormalization over the coherent band, and is not necessarily equal to the conventional renormalization factor at E_F .
- [23] T.A. Maier, M. Jarrell and D.J. Scalapino, Phys. Rev. B **74**, 094513 (2006).
- [24] M. Jarrell *et. al.*, Europhysics Letter, **56**, 563 (2001).
- [25] A. Comanac *et. al.*, Nature Physics, **4** 287 (2008).